

# Resolving Fermi surfaces with tensor networks

Quinten Mortier,<sup>1,\*</sup> Norbert Schuch,<sup>2,3</sup> Frank Verstraete,<sup>1</sup> and Jutho Haegeman<sup>1</sup>

<sup>1</sup>*Department of Physics and Astronomy, Ghent University, Krijgslaan 281, S9, 9000 Gent, Belgium*

<sup>2</sup>*Max-Planck-Institute of Quantum Optics, Hans-Kopfermann-Str. 1, 85748 Garching, Germany*

<sup>3</sup>*Munich Center for Quantum Science and Technology, Schellingstr. 4, 80799 München, Germany*

We show that Projected Entangled-Pair States (PEPS) are able to describe critical, fermionic systems exhibiting both 1d and 0d Fermi surfaces on a 2d lattice. In the thermodynamic limit, the energy precision as a function of the bond dimension improves as a power law, illustrating that an arbitrary precision can be obtained by increasing the bond dimension in a controlled manner. We also identify a non-trivial obstruction in the Gaussian and fermionic variant of PEPS, rooted in its topology and restricting its efficient applicability to models with a matching parity configuration.

## I. INTRODUCTION

In one spatial dimension, physically relevant states of quantum many-body systems with a local and gapped Hamiltonian can be represented efficiently by Matrix-Product States (MPS). A natural extension of this construction to higher dimensions was formulated in the form of Projected Entangled-Pair States (PEPS) [1] and both ansatzes thank their versatile applicability to an inherent area law of entanglement [2]. However, critical systems, with correlations following a power-law decay, can violate this area law in a logarithmic manner. Do tensor networks like MPS and PEPS then still represent efficient ansatzes for the relevant states of such critical models? In one dimension, this question was already answered in an affirmative way, concluding that even in the thermodynamic limit an arbitrary precision can be obtained by increasing the bond dimension in a controlled manner [3]. In this work, we aim to extend this claim to the two-dimensional case.

In fermionic systems, logarithmic violations of the area law of entanglement go hand in hand with the presence of Fermi surfaces [4, 5]. These discontinuities in the Green's functions manifest themselves already in translation invariant, quadratic models as continuous sets of zero energy modes in Fourier space. Therefore, we will focus on free-fermion systems with a Fermi surface. This allows for the application of the Gaussian and fermionic version of the PEPS ansatz (GfPEPS) [6], reducing the computational cost of the required simulations. We first show that GfPEPS in 1d can reproduce the aforementioned power-law improvement of the precision as a function of the bond dimension by considering the critical points of the Kitaev chain. Subsequently, 1d and 0d Fermi surfaces in 2d lattice systems are treated by considering the p-wave superconductor and Chern insulator, respectively. In both cases, we again obtain a power-law relation between bond dimension and precision in the thermodynamic limit (albeit with different exponents), indicating that PEPS (MPS) can describe gapless models and in particular Fermi surfaces of arbitrary dimensions.

We also observe that GfPEPS suffer from parity obstructions. Where general translation invariant, Gaussian states have a definite but arbitrary parity in the high-symmetry modes in Fourier space (*i.e.* the  $2^d$  (with  $d$  the spatial dimension)  $\mathbf{k}$  points that are invariant under inversion) and can therefore realize  $2^{2^d}$  parity configurations, this freedom is already exhausted in GfPEPS by fixing the parity in the zone center and its  $d$  neighboring high-symmetry  $\mathbf{k}$  modes, totaling only  $2^{d+1}$  possible parity configurations. In two (or more) spatial dimensions, this amounts to the existence of states that can not be approximated by GfPEPS as they have parity configurations that are unattainable for the GfPEPS ansatz. These typically occur in topologically non-trivial settings or when an incommensurate filling is considered, thus signaling some topologically rooted obstruction for GfPEPS in these cases.

## II. GAUSSIAN FERMIONIC PEPS

Consider a 2d lattice built up by a periodic repetition of  $N_1 \times N_2 = N$  unit cells, spanned by  $\mathbf{a}_1$  and  $\mathbf{a}_2$ . To each vertex we attribute  $f$  physical fermionic orbitals with creation (annihilation) operators  $a_{\mathbf{n}}^{j\dagger}$  ( $a_{\mathbf{n}}^j$ ) where  $\mathbf{n} = n_i \mathbf{a}_i$  with  $n_i = 0, \dots, N_i - 1$  is the site and  $j = 1, \dots, f$  the orbital index. Corresponding Majorana operators are denoted by  $c_{\mathbf{n}}^{2j-1} = a_{\mathbf{n}}^{j\dagger} + a_{\mathbf{n}}^j$  and  $c_{\mathbf{n}}^{2j} = -i(a_{\mathbf{n}}^{j\dagger} - a_{\mathbf{n}}^j)$ . Within this framework, a PEPS ansatz is obtained by first introducing four sets of virtual Majoranas per site:  $\{c_{\mathbf{n}}^{l,i_1}\}$ ,  $\{c_{\mathbf{n}}^{r,i_1}\}$ ,  $\{c_{\mathbf{n}}^{d,i_2}\}$  and  $\{c_{\mathbf{n}}^{u,i_2}\}$  with  $i_1 = 1, \dots, \chi_1$  and  $i_2 = 1, \dots, \chi_2$ . Next, a valence bond state  $\rho_{\text{in}}$  is constructed on the virtual level by entangling neighboring Majoranas in both directions (see Fig. 1). This is realized by placing the Majoranas in their joint vacuum[7]. Finally, the maximally entangled state is projected onto the physical level in a local way by the channel  $\mathcal{E} = \bigotimes_{\mathbf{n}} \mathcal{E}_{\mathbf{n}}^{\text{loc}}$ , yielding the (possibly mixed)  $\rho_{\text{out}} = \mathcal{E}(\rho_{\text{in}})$ . By increasing the number of virtual Majoranas, the ansatz can be enlarged and as the number of Majoranas can be different in each direction, the corresponding, effective bond dimensions,  $D_i = \sqrt{2}^{\chi_i}$ , can differ as well.

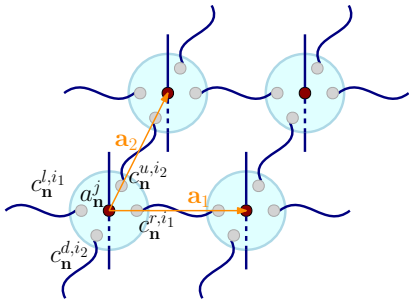


FIG. 1. Schematic of a GfPEPS on a 2d lattice with unit vectors  $\mathbf{a}_1$  and  $\mathbf{a}_2$ . Majorana modes (gray balls) are entangled (blue lines) to form a valence bond state which is locally projected by a Gaussian map (big blue circles) to the physical fermions (red balls).

As  $\rho_{\text{in}}$  is a free-fermion state, Gaussianity of the PEPS can be enforced by restricting the channel  $\mathcal{E}$  to be Gaussian [8, 9]. Not only can then both the input and the output state be fully described in terms of their real and anti-symmetric correlation matrices,  $\Gamma_{\mathbf{nm}}^{ij} = \frac{i}{2} \text{Tr}(\rho [c_{\mathbf{n}}^i, c_{\mathbf{m}}^j])$ , but there is also a link between both in the form of a Schur complement

$$\Gamma_{\text{out}} = A - B(D + \Gamma_{\text{in}}^{-1})^{-1}C. \quad (1)$$

Here,  $A = \bigoplus_{\mathbf{n}} A_{\mathbf{n}}^{\text{loc}}$  and analogous decompositions apply for  $B$ ,  $C$  and  $D$  with  $A_{\mathbf{n}}^{\text{loc}} \in \mathbb{R}^{2f \times 2f}$ ,  $B_{\mathbf{n}}^{\text{loc}} \in \mathbb{R}^{2f \times 2(\chi_1 + \chi_2)}$ ,  $C_{\mathbf{n}}^{\text{loc}} \in \mathbb{R}^{2(\chi_1 + \chi_2) \times 2f}$  and  $D_{\mathbf{n}}^{\text{loc}} \in \mathbb{R}^{2(\chi_1 + \chi_2) \times 2(\chi_1 + \chi_2)}$ . Furthermore,  $X = \begin{pmatrix} A & B \\ C & D \end{pmatrix}$  is anti-symmetric and  $XX^T \leq \mathbb{1}$  with the equality holding for a pure state.

For translation invariant Gaussian states, it is more convenient to work in Fourier space where these states can be described completely in terms of the Fourier transformed correlation matrix,  $G_{\mathbf{kq}}^{ij} = \frac{i}{2} \text{Tr}(\rho [d_{\mathbf{k}}^i, d_{\mathbf{q}}^{j\dagger}])$ . Herein,  $d_{\mathbf{k}}^i = \frac{1}{\sqrt{N}} \sum_{\mathbf{n}} e^{-i\mathbf{k}\cdot\mathbf{n}} c_{\mathbf{n}}^i$  is the Fourier transformed version of  $c_{\mathbf{n}}^i$  with momentum modes  $\mathbf{k} = \frac{k_i}{N_i} \mathbf{b}_i$  ( $k_i = 0, \dots, N_i - 1$  and  $\mathbf{b}_i$  the reciprocal lattice vectors). The Fourier transformed correlation matrix is anti-hermitian,  $GG^\dagger \leq \mathbb{1}$  (with the equality again holding for a pure state) and for translation invariant states  $G$  decomposes in diagonal blocks  $G = \bigoplus_{\mathbf{k}} G(\mathbf{k})$  with, for instance,

$$G_{\text{in}}(\mathbf{k}) = \begin{pmatrix} 0 & e^{i\mathbf{k}\cdot\mathbf{a}_1} \\ -e^{-i\mathbf{k}\cdot\mathbf{a}_1} & 0 \end{pmatrix}^{\oplus \chi_1} \oplus \begin{pmatrix} 0 & e^{i\mathbf{k}\cdot\mathbf{a}_2} \\ -e^{-i\mathbf{k}\cdot\mathbf{a}_2} & 0 \end{pmatrix}^{\oplus \chi_2} \quad (2)$$

for the input state. Assuming the PEPS and thus  $\mathcal{E}$  to be translation invariant so that  $\mathcal{E}_{\mathbf{n}}^{\text{loc}}$  is independent of  $\mathbf{n}$ , the transition matrix  $X$  decomposes in identical blocks yielding

$$G_{\text{out}}(\mathbf{k}) = A^{\text{loc}} - B^{\text{loc}}(D^{\text{loc}} - G_{\text{in}}(\mathbf{k}))^{-1}C^{\text{loc}}, \quad (3)$$

where the purity of the input state was used to replace  $G_{\text{in}}^{-1}(\mathbf{k})$ . Expressing the remaining inverse in Eq. (3) as the quotient of the adjugate and the determinant, one obtains that every entry of  $G_{\text{out}}(\mathbf{k})$  is the quotient of trigonometric polynomials of degree  $\leq 2\chi_i$  in the direction of  $\mathbf{b}_i$ .

### III. APPLICATION TO CRITICAL MODELS

#### A. Kitaev chain

We first apply the GfPEPS ansatz in 1d to illustrate that it can deal with critical models and exhibits a precision improvement that follows a power law as a function of the bond dimension in accordance with earlier results [3]. Consider therefore the 1d Kitaev chain of length  $N$  with periodic boundary conditions

$$H = -t \sum_{n=0}^{N-1} (a_n^\dagger a_{n+1} + h.c.) - \mu \sum_{n=0}^{N-1} a_n^\dagger a_n - \Delta \sum_{n=0}^{N-1} (a_n^\dagger a_{n+1}^\dagger + h.c.) \quad (4)$$

and assume  $t$  to be positive. For  $|\mu| > 2t$ , the system is in a trivial phase with the ground state reducing to a product state when  $\Delta = 0$  and all momentum modes filled (empty) when  $\mu > 2t$  ( $\mu < -2t$ ). For  $\Delta \neq 0$  and  $|\mu| < 2t$ , on the other hand, the system is in a chiral phase (with isolated Majoranas on both ends of the wire when the chain is cut). Critical lines lie at  $\mu = \pm 2t$  and at  $\Delta = 0$  when  $|\mu| < 2t$ . We optimized GfPEPS by minimizing their energy for both gapless and gapped parameter choices and for a number of virtual Majorana modes,  $\chi$ , ranging from 1 to 15. The resulting energy density error is displayed in Fig. 2. For the critical model, a power-law improvement of the precision is obtained in case of an odd number of virtual Majoranas. An even  $\chi$ , on the other hand, yields a saturating profile for  $\Delta e$ . Similar observations apply in the chiral phase but with an even faster convergence as the area law of entanglement is not violated. In particular, the chiral phase exhibits an exact MPS ground state with  $\chi = 1$  at the point  $\Delta = t, \mu = 0$ . Finally, optimization in the trivial phase results in profiles similar to those in the chiral phase but with the odd and even  $\chi$  curves interchanged. In Section IV B we will show that the number of virtual Majorana modes determines the parity configuration of the GfPEPS ansatz and that this configuration should be identical to the one of the targeted state. Furthermore, there is link between the exact parity configuration and the topological features of the model. Here, this is reflected by the fact that an even number of Majorana modes should be used in the trivial phase while an odd  $\chi$  should be utilized in the topological region, in accordance with the relevant underlying physics with isolated Majorana edge modes in the topological phase.

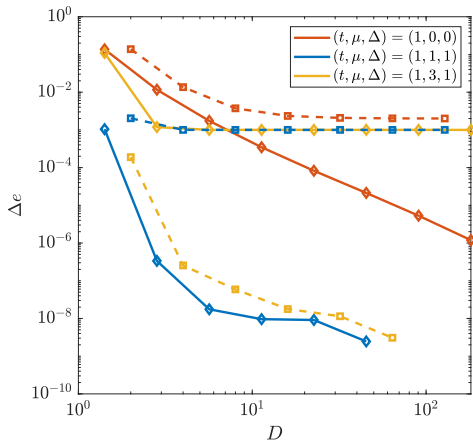


FIG. 2. Energy density error of optimized GfPEPS for the Kitaev chain as a function of the bond dimension  $D = \sqrt{2}^\chi$  with  $\chi$  the number of virtual Majorana modes. Dashed lines are used for an even  $\chi$  whereas full lines denote an odd number of virtual Majorana modes. GfPEPS with a  $\chi$  that satisfies the parity constraints can approximate the exact solution with an arbitrary precision if the bond dimension is increased according to a power law for the gapless model ( $t = 1, \mu = 0, \Delta = 0$ ) and with an even smaller  $D$  in gapped phases. In contrast, the precision of parity obstructed GfPEPS saturates.

### B. p-Wave superconductor

Switching to 2d, the analogue of the Kitaev chain is the p-wave superconductor on a square lattice with

$$\begin{aligned}
 H &= H_t + H_\mu + H_\Delta \\
 H_t &= -t \sum_{\mathbf{n}} (a_{\mathbf{n}}^\dagger a_{\mathbf{n}\rightarrow} + a_{\mathbf{n}}^\dagger a_{\mathbf{n}\uparrow} + h.c.) \\
 H_\mu &= -\mu \sum_{\mathbf{n}} a_{\mathbf{n}}^\dagger a_{\mathbf{n}} \\
 H_\Delta &= -\Delta \sum_{\mathbf{n}} (a_{\mathbf{n}}^\dagger a_{\mathbf{n}\rightarrow}^\dagger + i a_{\mathbf{n}}^\dagger a_{\mathbf{n}\uparrow}^\dagger + h.c.)
 \end{aligned} \tag{5}$$

where  $\mathbf{n}_{\rightarrow, \uparrow} = \mathbf{n} + \mathbf{a}_{1,2}$  with  $\mathbf{a}_{1,2}$  the unit vectors in the horizontal and vertical direction and where the phase difference between the two spatial components of the pairing term is necessary to open a gap. Again taking  $t > 0$ , topologically trivial regions are found when  $|\mu| > 4t$ . For  $0 < \mu < 4t$ , one obtains a chiral phase with Chern number  $C = -1$ , whereas  $-4t < \mu < 0$  yields  $C = +1$ . Critical lines lie in between and at analogous places as for the 1d Kitaev chain. For  $\Delta = 0$  and  $-4t < \mu < 4t$  the model exhibits a 1d Fermi surface. The applicability of (G)fPEPS to models with a Fermi surface was hence studied in the point where  $\mu = \Delta = 0$ , *i.e.* the point where the p-wave superconductor reduces to the square lattice hopping model. Just as for the Kitaev chain, parity constraints require an odd number of virtual Majorana modes in this point. Furthermore, we will show in

Section IV C that (again due to parity considerations) simulations for the hopping model are more stable when it is approached from its anisotropic analogue where  $H_t$  is replaced by

$$H_t = - \sum_{\mathbf{n}} (t_x a_{\mathbf{n}}^\dagger a_{\mathbf{n}\rightarrow} + t_y a_{\mathbf{n}}^\dagger a_{\mathbf{n}\uparrow} + h.c.) . \tag{6}$$

Systematically reducing  $\frac{t_y}{t_x}$  to 1 and using GfPEPS solutions at higher anisotropies as an initial guess for simulations at a lower  $\frac{t_y}{t_x}$ , an optimized GfPEPS for the isotropic hopping model was obtained. The energy density error hereof as a function of both the geometric mean of the bond dimensions,  $\sqrt{D_1 D_2}$ , and the linear system size,  $L = \sqrt{N} = N_1 = N_2$ , is displayed in Fig. 3. The bottom panel shows that by increasing the system size and keeping  $\sqrt{D_1 D_2}$  fixed, the energy error saturates, indicating that the thermodynamic limit is probed for the bond dimension under consideration. For the largest system size, this is the case for all the considered bond dimensions and the curve for  $L = 1000$  in the top panel can hence be interpreted as the energy density error as a function of  $\sqrt{D_1 D_2}$  in the thermodynamic limit. Herein, (the onset of) a power-law improvement of the precision can clearly be discerned. We conclude that, just as in the 1d case, 2d models with 1d Fermi surfaces can (even in the thermodynamic limit) be approximated by PEPS with an arbitrary precision by increasing the bond dimension in a controlled way [10].

### C. Chern insulator

Where the previous example demonstrates the applicability of (G)fPEPS to 2d models with a 1d Fermi surface, a square lattice Chern insulator with one or two point-like, 0d Fermi surfaces is considered next. In Fourier space, the Hamiltonian hereof is given by

$$H = \sum_{\mathbf{k}} \begin{pmatrix} a_{\mathbf{k}}^{1\dagger} & a_{\mathbf{k}}^{2\dagger} \end{pmatrix} \mathbf{h}(\mathbf{k}) \cdot \boldsymbol{\sigma} \begin{pmatrix} a_{\mathbf{k}}^1 \\ a_{\mathbf{k}}^2 \end{pmatrix} \tag{7}$$

with  $\mathbf{h}(\mathbf{k}) = (\sin k_1, \sin k_2, \Delta + \cos k_1 + \cos k_2)^T$  and  $\boldsymbol{\sigma}$  containing the Pauli matrices. For  $|\Delta| > 2$ , this model is topologically trivial, while a chiral phase with Chern number  $C = 1$  ( $C = -1$ ) is found when  $0 < \Delta < 2$  ( $-2 < \Delta < 0$ ). Critical points are hence located at  $\Delta = -2, 0, 2$ . At the boundaries between trivial and chiral phases, the dispersion relation displays only one 0d Fermi surface, located at the Brillouin zone center when  $\Delta = -2$  and at  $(\pi, \pi)$  when  $\Delta = 2$ . The dispersion around this critical mode is linear, *i.e.* it exhibits a Dirac cone. The critical point between the two chiral phases, on the other hand, has two Dirac cones at  $(0, \pi)$  and  $(\pi, 0)$  and is therefore expected to contain more entanglement than the other critical points. GfPEPS were optimized for both types of critical models (namely for  $\Delta = 0$  and  $\Delta = 2$ ) and, as will be discussed in the Section IV B,

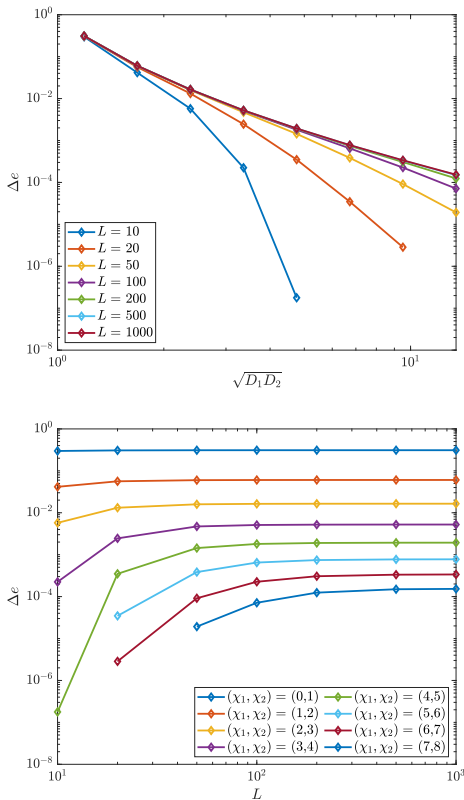


FIG. 3. Energy density error of optimized GfPEPS for the 2d square lattice hopping model ( $t = 1, \mu = 0, \Delta = 0$ ) as a function of both the geometric mean of the bond dimensions  $\sqrt{D_1 D_2}$  (top panel) and the linear system size  $L$  (bottom panel). The thermodynamic limit was clearly probed for all bond dimensions when  $L = 1000$  and the onset of a power law can be discerned in the top panel. The isotropic hopping model was probed by approaching it from an anisotropic hopping model with the anisotropy systematically dropping down to  $10^{-5}$  in the displayed results.

an even number of virtual Majorana modes is used in both directions to reproduce the exact parity configuration. The resulting energy density errors are displayed in Fig. 4 and 5. Again, the bottom panels show that the thermodynamic limit is probed for all bond dimensions when  $L = 1000$  and even though there is no violation of the area law of entanglement, (the onset of) a power-law improvement of the precision can be discerned from the top panels. However, the exponents are different, indicating that fewer Dirac cones require a lower bond dimension to obtain the same precision. Furthermore, the precision improvement is in both cases faster than that of the square lattice hopping model which does violate the area law of entanglement. We conclude that in all the considered cases, the energy precision increases at least according to a power-law as a function of the bond dimension and thus that GfPEPS can deal with both 1d and 0d Fermi surfaces, even in the thermodynamic limit.

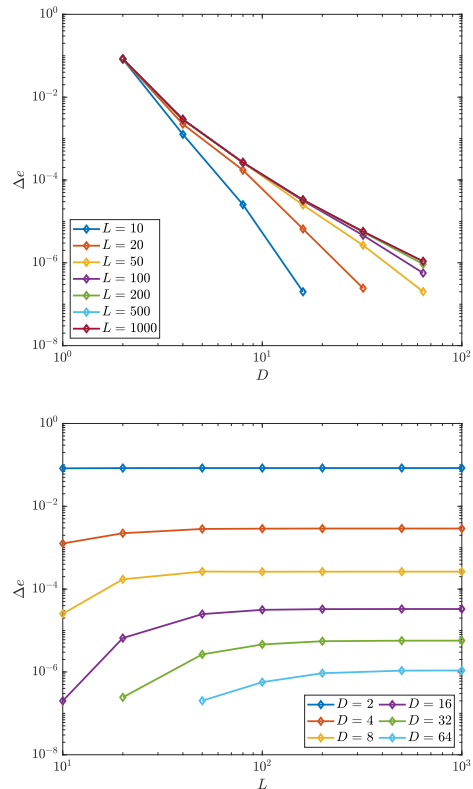


FIG. 4. Energy density error of optimized GfPEPS for a critical Chern insulator on a 2d square lattice with two Dirac cones ( $\Delta = 0$ ) as a function of both the bond dimension  $D = \sqrt{2}^{X_1} = \sqrt{2}^{X_2}$  (top panel) and the linear system size  $L$  (bottom panel). The thermodynamic limit was clearly probed for all bond dimensions when  $L = 1000$  and the onset of a power law can be discerned in the top panel.

## IV. PARITY OBSTRUCTION

### A. Observation

Performing GfPEPS optimizations in two spatial dimensions, we encountered parity obstructions. Already for the p-wave superconductor with  $\Delta = 0$  and  $0 < |\mu| < 4t$ , one faces a problematic target state. Indeed, the high-symmetry modes in the square lattice Brillouin zone are located at  $(0, 0)$ ,  $(0, \pi)$ ,  $(\pi, 0)$  and  $(\pi, \pi)$ . When a chemical potential is present, three of these modes have the same filling while the fourth is different. Fig. 6 illustrates that this is not compatible with the GfPEPS ansatz. Indeed, optimizing GfPEPS with all possible combinations of even and odd numbers of virtual Majoranas, none succeeds in reproducing the exact filling (and thus parity) in all of the high-symmetry  $\mathbf{k}$  points. This results in errors on correlation functions, energies, *etc.* One could try to avoid these problems by using only odd length lattices as the problematic  $\mathbf{k}$  points are no longer sampled then. However, the

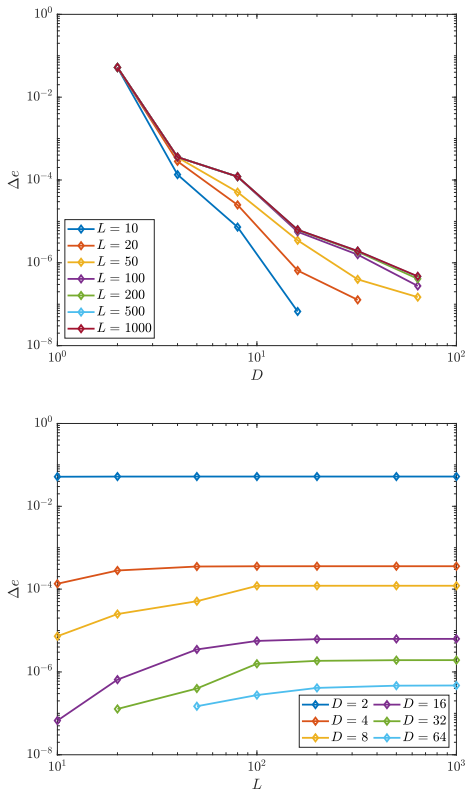


FIG. 5. Energy density error of optimized GfPEPS for a critical Chern insulator on a 2d square lattice with one Dirac cone ( $\Delta = 2$ ) as a function of both the bond dimension  $D = \sqrt{2}^{\chi_1} = \sqrt{2}^{\chi_2}$  (top panel) and the linear system size  $L$  (bottom panel). The thermodynamic limit was clearly probed for all bond dimensions when  $L = 1000$  and a power law improvement of the precision can be discerned in the top panel.

regularity of  $G(\mathbf{k})$  will also induce errors in the vicinity of the high-symmetry modes, thus requiring a higher bond dimension to really overcome the problem. Furthermore, this approach typically suffers from numerical instability. Similar remarks apply when the relative importance of the problematic points is reduced by directly working in the thermodynamic limit (with the additional complication that the energy density in the thermodynamic limit can only be computed exactly in 1d so that it becomes harder to solve the variational problem in higher dimensions).

### B. Obstruction

In the previous section we observed that certain parity configurations are unattainable for the GfPEPS ansatz. The parity structures that they can realize, on the other hand, are determined by the number of virtual Majorana modes in each direction and the parity

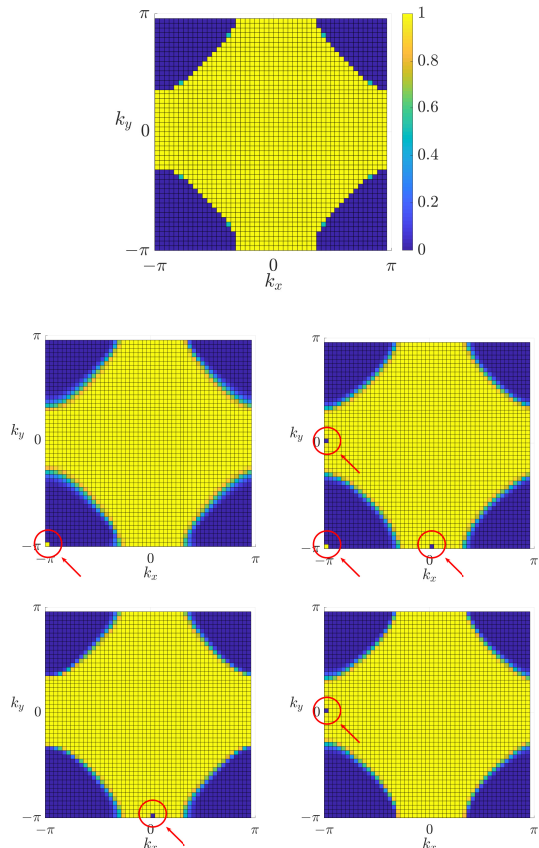


FIG. 6. Modal occupation in Fourier space for a p-wave superconductor with  $t = 1$ ,  $\mu = 1$  and  $\Delta = 0$  in the exact ground state (top panel), in a numerically optimized GfPEPS with (4, 4) (middle left), (5, 5) (middle right), (4, 5) (bottom left) and (5, 4) (bottom right) virtual Majorana modes. The GfPEPS projection  $\mathcal{E}$  was always chosen to be parity changing so that the zone center is occupied. As indicated by the red arrows, none of the GfPEPS succeeds in reproducing the exact parity structure in all of the high-symmetry  $\mathbf{k}$  modes.

conserving/changing nature of  $\mathcal{E}$ . The link between the  $\{\chi_i\}$  and the GfPEPS parity configuration originates from the input state  $\rho_{\text{in}}$ . As real-space correlation matrices are real-valued, their Fourier transformed analogues have the property that  $G(-\mathbf{k}) = G^*(\mathbf{k})$ . This implies that  $G(\mathbf{k})$  is real and anti-symmetric in points where  $\mathbf{k} = -\mathbf{k}$ . Consequently,  $G(\mathbf{k})$  can be interpreted as an ordinary correlation matrix. The specific form of  $G_{\text{in}}(\mathbf{k})$  even amounts to a definite parity  $P_{\mathbf{k}} = \left(\prod_{i_1} i d_{\mathbf{k}}^{i_1} d_{\mathbf{k}}^{i_1}\right) \left(\prod_{i_2} i d_{\mathbf{k}}^{i_2} d_{\mathbf{k}}^{i_2}\right)$  for the input state in the high-symmetry points. Indeed,  $\langle P_{\mathbf{k}} \rangle_{\text{in}} = \text{Pf}(G_{\text{in}}(\mathbf{k})) = (e^{i\mathbf{k}\cdot\mathbf{a}_1})^{\chi_1} (e^{i\mathbf{k}\cdot\mathbf{a}_2})^{\chi_2}$  so that the center of the Brillouin zone always has an even parity,  $\langle P_0 \rangle_{\text{in}} = 1$ , while for the other high-symmetry points  $\langle P_{\frac{\mathbf{b}_i}{2}} \rangle_{\text{in}} = (-1)^{\chi_i}$  and  $\langle P_{\frac{\mathbf{b}_1 + \mathbf{b}_2}{2}} \rangle_{\text{in}} = (-1)^{\chi_1 + \chi_2}$ . A  $\frac{\mathbf{b}_i}{2}$  jump in Fourier space thus corresponds to an extra factor

$(-1)^{\chi_i}$ . Remarkably, this virtual parity configuration is lifted to the physical level by the Gaussian projection  $\mathcal{E}$ . Indeed, in order for the full PEPS ansatz to have a fixed global parity, the projectors,  $\mathcal{E}_{\mathbf{n}}^{\text{loc}}$ , are designed to be parity conserving (changing) [6]. Combining this with their local and translation invariant nature, GfPEPS have the same (opposite) parity configuration as the valence bond state in the high-symmetry points, *i.e.*  $\langle P_{\mathbf{k}} \rangle_{\text{out}} = \langle (-1)^{\sum_j a_{\mathbf{k}}^{j\dagger} a_{\mathbf{k}}^j} \rangle_{\text{out}} = \text{Pf}(G_{\text{out}}(\mathbf{k})) = \pm \langle P_{\mathbf{k}} \rangle_{\text{in}}$  when  $\mathbf{k} = -\mathbf{k}$ . We conclude that GfPEPS can only realize  $2^d \times 2$  (even/odd  $\chi$  in each direction and parity conserving/changing  $\mathcal{E}$ ) parity configurations while for an arbitrary Gaussian state, there are  $2^{2^d}$  possible configurations. Parity obstructions thus exist for GfPEPS in all spatial dimensions larger than one. For a proof hereof solely based on the Schur complements in Eq. (1), we refer to Appendix A.

What do the specific parity configurations of GfPEPS entail for their applicability to systems with Fermi surfaces? Non-degenerate Fermi surfaces represent boundaries between regions with different fillings and thus parities. In this way, their shapes determine the parity structure of the targeted state and are therefore constrained if GfPEPS optimization is envisioned. Consider, for instance, a general translation invariant free-fermion Hamiltonian with  $f$  physical fermions per site

$$H = \sum_{\substack{\mathbf{m}, \mathbf{n} \\ i, j=1, \dots, f}} a_{\mathbf{m}}^{i\dagger} H_{\mathbf{m}\mathbf{n}}^{ij} a_{\mathbf{n}}^j = \sum_{\mathbf{k}} \varepsilon^i(\mathbf{k}) b_{\mathbf{k}}^{i\dagger} b_{\mathbf{k}}^i \quad (8)$$

where the diagonalized form is obtained by first Fourier transforming the operators and then unitarily transforming them according to  $b_{\mathbf{k}}^i = U^{ij}(\mathbf{k}) a_{\mathbf{k}}^j$ . Every connected set of zero-energy points represents a Fermi surface with the sign of one of the energies switching across. The ground state filling of the  $b_{\mathbf{k}}^i$  modes will switch as well, thus altering the parity  $\langle P_{\mathbf{k}}^b \rangle_{\text{ex}} = \langle (-1)^{\sum_j b_{\mathbf{k}}^{j\dagger} b_{\mathbf{k}}^j} \rangle_{\text{ex}} = \langle (-1)^{\sum_j a_{\mathbf{k}}^{j\dagger} a_{\mathbf{k}}^j} \rangle_{\text{ex}} = \langle P_{\mathbf{k}}^a \rangle_{\text{ex}}$ . Fermi surfaces should therefore be organized in such a way that an admissible parity configuration is obtained for GfPEPS to be applicable.

### C. Possible remedies

We showed that states with inadmissible Fermi surface morphologies exist in spatial dimensions larger than one. Is it possible to resolve these issues or to approximate problematic states coming from a direction that does not pose difficulties for GfPEPS? Put differently, can we come up with alterations to inadmissible target states (and thus to their parent Hamiltonians) that resolve problematic parity configurations? Perhaps the most evident solution for an inadmissible Fermi surface consists of altering the Hamiltonian so that the Fermi surface is slightly deformed, making the model compatible with the GfPEPS ansatz. A particular example hereof is

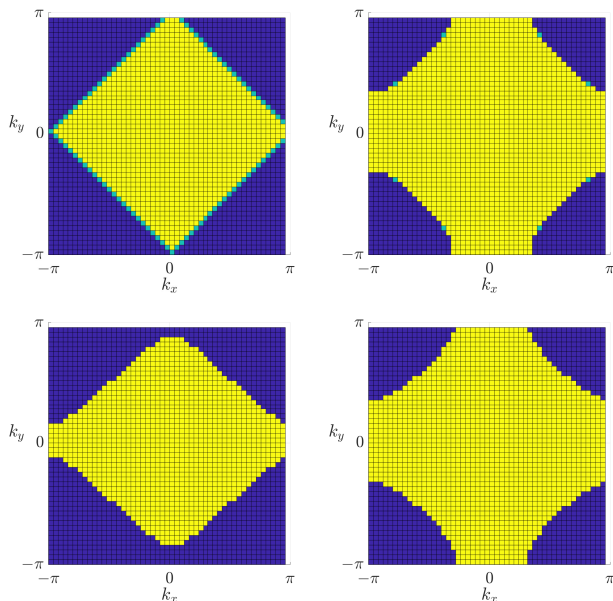


FIG. 7. Illustration of the influence of anisotropies on the Fermi surfaces in a hopping model with both commensurate and incommensurate filling. Parameter choices:  $t_x = t_y = 1$ ,  $\mu = 0$  (top left),  $t_x = t_y = 1$ ,  $\mu = 1$  (top right),  $t_x = 1$ ,  $t_y = 1.1$ ,  $\mu = 0$  (bottom left),  $t_x = 1$ ,  $t_y = 1.1$ ,  $\mu = 1$  (bottom right). While a slight Fermi surface deformation leads to an admissible parity configuration in the commensurate model, this is not the case when  $\mu \neq 0$ .

the square lattice hopping model from Section III B. Herein, the Fermi surface is a square connecting the  $(0, \pi)$  and  $(\pi, 0)$  points (see Fig. 7) and choosing to fill one of these modes while leaving the other empty, an attainable GfPEPS approximation without errors for the ground state energy density can be put forward. However, adding even the slightest chemical potential immediately yields an inadmissible target state, thus making the direct application of GfPEPS unstable. Therefore, it is better to optimize GfPEPS for the anisotropic hopping model. Indeed, as Fig. 7 shows these have a fully admissible parity structure when  $t_y \neq t_x$  and in this way we can get arbitrarily close to the isotropic point without obstruction. A slight Fermi surface deformation thus allows to circumvent the aforementioned problems and systematically decreasing the anisotropy, the isotropic model can be approached in a stable way. Note however that when the ground state for  $\mu \neq 0$  is targeted, Fermi surface deformation does not work. Indeed, these models require a finite anisotropy to yield an admissible parity configuration and can as such not be approached by using a stabilizing Fermi surface deformation (see Fig. 7). The fact that incurable Fermi surface topologies occur when  $\mu \neq 0$  also shows some similarities with previously encountered problems for tensor networks approximating states with an incommensurate filling [11].

Next, we consider the opening of a gap as a way to resolve inadmissible, critical models. One way to open a gap is by introducing superconducting pairing terms and thus breaking  $U(1)$  symmetry. In this way the general Hamiltonian of Eq. (8) is lifted to the broader category of quadratic models described by a Bogoliubov-de Gennes (BdG) type Hamiltonian

$$H = \frac{1}{2} \sum_{AB} \Upsilon_A^\dagger H_{\text{BdG}}^{AB} \Upsilon_B + \tilde{E} \quad (9)$$

where  $\tilde{E}$  is an energy offset,  $\Upsilon = \left( \{a_{\mathbf{n}}^i\}_{\mathbf{n}}^i, \{a_{\mathbf{n}}^{i\dagger}\}_{\mathbf{n}}^i \right)^T$  is the Nambu spinor and where the  $A, B$  labels discern between its upper and lower half. Due to the manifest particle hole symmetry,  $(\sigma_1 \otimes \mathbb{1}) H_{\text{BdG}}^T (\sigma_1 \otimes \mathbb{1}) = -H_{\text{BdG}}$ , this Hamiltonian can be rewritten as

$$H_{\text{BdG}} = \begin{pmatrix} \Xi & \Delta \\ -\Delta^* & -\Xi^T \end{pmatrix}, \quad \Xi = \Xi^\dagger, \quad \Delta = -\Delta^T. \quad (10)$$

Further assuming translation invariance, it is again more convenient to work in Fourier space where

$$H = \frac{1}{2} \sum_{\mathbf{k}} \Upsilon_{\mathbf{k}}^\dagger \begin{pmatrix} \Xi(\mathbf{k}) & \Delta(\mathbf{k}) \\ -\Delta^*(-\mathbf{k}) & -\Xi^T(-\mathbf{k}) \end{pmatrix} \Upsilon_{\mathbf{k}} + \tilde{E} \quad (11)$$

with  $\Upsilon_{\mathbf{k}} = \left( \{a_{\mathbf{k}}^i\}^i, \{a_{-\mathbf{k}}^{i\dagger}\}^i \right)^T$ . Here, a Bogoliubov transformation  $\tilde{\Upsilon}_{\mathbf{k}} = U(\mathbf{k})\Upsilon_{\mathbf{k}}$  with  $U(\mathbf{k}) = \begin{pmatrix} U^{11}(\mathbf{k}) & U^{12}(\mathbf{k}) \\ U^{12*}(-\mathbf{k}) & U^{11*}(-\mathbf{k}) \end{pmatrix}$  can be utilized to diagonalize the Hamiltonian with

$$\begin{aligned} H &= \frac{1}{2} \sum_{\mathbf{k}} \tilde{\Upsilon}_{\mathbf{k}}^\dagger \begin{pmatrix} e(\mathbf{k}) & 0 \\ 0 & -e(-\mathbf{k}) \end{pmatrix} \tilde{\Upsilon}_{\mathbf{k}} + \tilde{E} \\ &= \sum_{\mathbf{k}, i} e^i(\mathbf{k}) \tilde{a}_{\mathbf{k}}^{i\dagger} \tilde{a}_{\mathbf{k}}^i - \frac{1}{2} \sum_{\mathbf{k}, i} e^i(\mathbf{k}) + \tilde{E}. \end{aligned} \quad (12)$$

Note that the full spectrum is symmetric around zero because of the particle hole symmetry. This allows to construct the Bogoliubov transformation so that  $e^i(\mathbf{k}) \geq 0$ . Consequently, the ground state filling of all modes can be set equal to zero and thus  $\langle \tilde{P}_{\mathbf{k}} \rangle_{\text{ex}} = \langle (-1)^{\sum_i \tilde{a}_{\mathbf{k}}^{i\dagger} \tilde{a}_{\mathbf{k}}^i} \rangle_{\text{ex}} = 1$ . In the high-symmetry points, this parity can be linked to the parity in terms of the original operators. Indeed, the Fourier transformed correlation matrices in both operator bases are related via  $G_{\text{ex}}(\mathbf{k}) = Z(\mathbf{k})\tilde{G}_{\text{ex}}(\mathbf{k})Z^\dagger(\mathbf{k})$  with  $Z(\mathbf{k}) = VU^\dagger(\mathbf{k})V^{-1}$  and  $V$  the constant matrix transforming the Nambu spinor in the  $\tilde{a}_{\mathbf{k}}^i$  operators. As  $Z(\mathbf{k})$  is real and orthogonal in the high-symmetry  $\mathbf{k}$  points (due to the increased symmetry in  $U(\mathbf{k})$ ), one obtains that  $\langle P_{\mathbf{k}} \rangle_{\text{ex}} = \text{Pf}(G_{\text{ex}}(\mathbf{k})) = \text{Pf}(Z(\mathbf{k})\tilde{G}_{\text{ex}}(\mathbf{k})Z^T(\mathbf{k})) = \det(Z) \text{Pf}(\tilde{G}_{\text{ex}}(\mathbf{k})) = \det(U(\mathbf{k}))$ . Opening a gap by

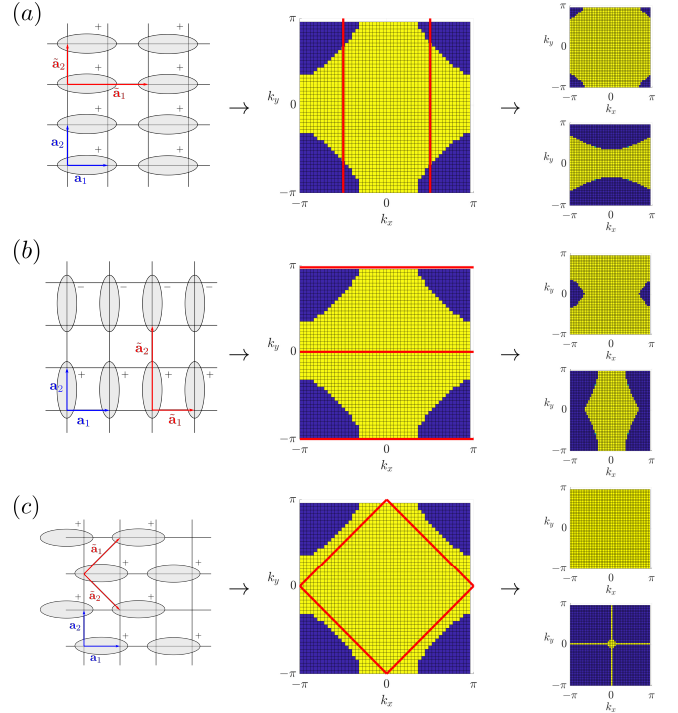


FIG. 8. Illustration of the influence of blocking sites together on dispersion relations and Fermi surfaces in a p-wave superconductor ( $t = \mu = 1$  and  $\Delta = 0$ ) for (a) a horizontal blocking without extra phases (upper panel), (b) a vertical blocking with an extra phase,  $(-1)^y$ , with  $y$  the new vertical index and (c) for a diagonal blocking without extra phase. The corresponding Brillouin zone tessellations are indicated in red. The new Fermi surfaces clearly correspond to the original, cut along the tessellation and with the addition of an appropriate shift.

continuously introducing pairing terms and hence smoothly modifying  $U(\mathbf{k})$  without changing the non-superconducting terms will therefore never result in an altered parity structure. Put differently, solely opening a gap by breaking  $U(1)$  symmetry will never change the parity configuration that was already present in the gapless model. Hamiltonians with an inadmissible Fermi surface morphology will therefore remain inadmissible in a superconducting phase. This was also observed in simulations for the p-wave superconductor in its chiral phases. Even for high  $\Delta$  values, the exact parity configuration remains inadmissible thus complicating an efficient GfPEPS application.

As opening a gap by breaking  $U(1)$  symmetry proved to be unfruitful, we now look at the possibility of opening a gap by breaking translation invariance. However, in order to maintain the Fourier space approach used until now, we will break translation invariance in a periodic manner (e.g. introducing an ABAB structure in 1d with a staggered chemical potential) and block the fermions in

one unit cell together. Therefore, the influence of blocking will be examined first. Blocking sites together generally comes down to replacing the primitive unit cell vectors  $\{\mathbf{a}_i\}$  by linear combinations hereof, thus enlarging the unit cell. In Fourier space, this corresponds to a tessellation of the first Brillouin zone into smaller parallelograms. The energy bands of the blocked model then correspond to the original dispersion relation cut along the tessellation and shifted into the new Brillouin zone. Furthermore, the tessellation can be translated along  $\pm \frac{\mathbf{b}_i}{2}$  by adding an appropriate, extra phase to the blocked operators. However, as illustrated in Fig. 8 for the p-wave superconductor with  $t = \mu = 1$  and  $\Delta = 0$ , this approach is in general not able to circumvent problematic parity configurations. Let us therefore examine the actual breaking of translation invariance. Consider, for instance, again the p-wave superconductor, omit the pairing terms (as these do not influence the parity structure) and implement a staggered blocking so that  $b_{\mathbf{x}}^1 = a_{(x+y, x-y)}$  and  $b_{\mathbf{x}}^2 = a_{(x+y+1, x-y)}$ , equivalent to the new lattice unit vectors  $\tilde{\mathbf{a}}_1 = \mathbf{a}_1 + \mathbf{a}_2$  and  $\tilde{\mathbf{a}}_2 = \mathbf{a}_1 - \mathbf{a}_2$ . Blocking in this way, the Brillouin zone is tessellated along the Fermi surface of the model when  $\mu = 0$  (see also Fig. 8(c)) and the Hamiltonian in the new operators is given by

$$\begin{aligned} H &= H_t + H_\mu \\ &= -t \sum_{\mathbf{x}} (b_{\mathbf{x}}^{1\dagger} b_{\mathbf{x}}^2 - b_{\mathbf{x}}^{1\dagger} b_{\mathbf{x}_\downarrow}^2 + b_{\mathbf{x}}^{2\dagger} b_{\mathbf{x}_\uparrow}^1 \\ &\quad - b_{\mathbf{x}}^{2\dagger} b_{\mathbf{x}_\downarrow}^1 + h.c.) - \mu \sum_{\mathbf{x}} (b_{\mathbf{x}}^{1\dagger} b_{\mathbf{x}}^1 + b_{\mathbf{x}}^{2\dagger} b_{\mathbf{x}}^2) \quad (13) \\ &= \sum_{\mathbf{k}} \begin{pmatrix} b_{\mathbf{k}}^1 \\ b_{\mathbf{k}}^2 \end{pmatrix}^\dagger \begin{pmatrix} -\mu & \varepsilon_t(\mathbf{k}) \\ \varepsilon_t^*(\mathbf{k}) & -\mu \end{pmatrix} \begin{pmatrix} b_{\mathbf{k}}^1 \\ b_{\mathbf{k}}^2 \end{pmatrix} \end{aligned}$$

where  $\varepsilon_t(\mathbf{k}) = -t(1 + e^{ik_x})(1 + e^{ik_y})$  and with the energy bands given by  $e(\mathbf{k}) = -\mu \pm |2t \cos \frac{k_x}{2} \cos \frac{k_y}{2}|$  (indeed corresponding to shifted versions of the original dispersion cut along the tessellation). Translation invariance of the original model can be broken by adding a staggered chemical potential  $\tilde{\mu}$  in the new  $x$  direction. The dispersion relation then becomes

$$e(\mathbf{k}) = -\mu \pm \sqrt{\tilde{\mu}^2 + \left(4t \sin \frac{k_x}{2} \sin \frac{k_y}{2}\right)^2} \quad (14)$$

with a gap opening due to  $\tilde{\mu}$  when  $\mu = 0$ , thus resolving the problematic Fermi surface morphology. However, when  $\mu \neq 0$ , a gapped model can only be found when a finite  $\tilde{\mu}$  is utilized. *I.e.* just as for Fermi surface deformation, opening a gap by breaking translation invariance only yields an admissible parity structure when the original model was already a borderline case.

Finally, one could also consider a finite temperature, systematically decreasing to zero, to resolve parity obstructions. Not only does this approach relax the constraint that  $XX^T = 1$  for pure GfPEPS but the

targeted state also no longer has a fixed parity configuration. However, for small temperatures, we found that the strong tendency of the GfPEPS to fill (vacate) negative (positive) energy states makes  $XX^T \approx 1$ , thus implementing the hard parity arrangement of the GfPEPS nonetheless. Again, one could say the lack of a direct immediacy of states with an admissible parity structure precludes the efficient use of GfPEPS.

## V. CONCLUSIONS

We studied whether projected entangled-pair states can be used to describe critical systems exhibiting Fermi surfaces. This question was answered in an affirmative way. Indeed, the Gaussian and fermionic version of the PEPS ansatz was successfully applied to 2d free-fermion systems with both 1d and 0d Fermi surfaces. More specifically, for the former we considered a critical point of the p-wave superconductor and observed that in the thermodynamic limit the precision of the GfPEPS approximation increased according to a power law as a function of the bond dimension. This is the 2d extension of earlier results hereabout in 1d, that were also reproduced for the gapless Kitaev chain. Furthermore, 0d Fermi surfaces exhibiting Dirac cones were also shown to pose no difficulties for PEPS as the energy precision for the exemplary, critical Chern insulator models also increased according to a power law but with even higher exponents.

We also found that in two and higher spatial dimensions, some states can not be targeted efficiently by GfPEPS as the exact parity configuration can not be reproduced. This typically occurs for topologically non-trivial states or in case of an incommensurate filling, signaling a topologically rooted obstruction for GfPEPS. These parity obstructions exist for critical and gapped states alike, and thus add an important caveat to previous studies based on GfPEPS or, equivalently, Grassmann tensor networks, for example those discussing their applicability to the description of chiral phases [12–18]. We were able to overcome these issues in a number of relevant cases, for instance, by slightly deforming the Fermi surface. When this approach failed, we demonstrated the impossibility to overcome the encountered difficulties also by blocking, opening a gap or even adding a finite temperature. Beyond what is discussed in the paper, we also looked at the ground states of graphene and the Haldane model on a (blocked) hexagonal lattice and found that GfPEPS also experience difficulties in approximating these, even though their parity configuration poses no problem. Consequently, it is possible that there are more obstructions for GfPEPS beyond those that we encountered here. Therefore, an interesting direction to follow up is the general identification and solution of these

obstructions, for instance, coming up with an arsenal of alterations to problematic models that are capable of resolving parity (and other) obstructions. Additionally, an important open question remains if these obstructions are solely present in Gaussian PEPS or also in the more general fermionic PEPS ansatz, and how this is related to the reduction of symmetry classifications for free fermion systems when interactions are added [19].

## ACKNOWLEDGMENTS

We would like to thank Erez Zohar and Ignacio Cirac for inspiring discussions. This work has received support from the European Research Council (ERC) under the European Union's Horizon 2020 program (grant agreement No. 715861 (ERQUAF), 647905 (QUTE) and 636201 (WASCOSYS)) and from the DFG (German Research Foundation) under Germany's Excellence Strategy (EXC2111-390814868).

\* quinten.mortier@ugent.be

- [1] F. Verstraete and J. I. Cirac, Phys. Rev. A **70**, 060302 (2004), arXiv:quant-ph/0311130.
- [2] M. M. Wolf, F. Verstraete, M. B. Hastings, and J. I. Cirac, Phys. Rev. Lett. **100**, 070502 (2008), arXiv:0704.3906.
- [3] F. Verstraete and J. I. Cirac, Physical Review B **73** (2006), 10.1103/physrevb.73.094423, arXiv:cond-mat/0505140.
- [4] M. M. Wolf, Phys. Rev. Lett. **96**, 010404 (2006), arXiv:quant-ph/0503219.
- [5] D. Gioev and I. Klich, Phys. Rev. Lett. **96**, 100503 (2006), arXiv:quant-ph/0504151.
- [6] C. V. Kraus, N. Schuch, F. Verstraete, and J. I. Cirac, Phys. Rev. A **81**, 052338 (2010), arXiv:0904.4667.
- [7] A valence bond state with maximally entangled bonds between full virtual fermions  $\alpha_n^{j_1}$  (left),  $\beta_n^{j_1}$  (right),  $\gamma_n^{j_2}$  (down) and  $\delta_n^{j_2}$  (up) ( $j_1 = 1, \dots, \xi_1$ ,  $j_2 = 1, \dots, \xi_2$ ) can be obtained by applying the horizontal,  $H_n^{j_1} = \frac{1}{\sqrt{2}} \left( 1 + \beta_n^{j_1 \dagger} \alpha_n^{j_1 \dagger} \right)$ , and vertical,  $V_n^{j_2} = \frac{1}{\sqrt{2}} \left( 1 + \delta_n^{j_2 \dagger} \gamma_n^{j_2 \dagger} \right)$ , entanglers to the virtual vacuum yielding

$$G_{\text{in}}(\mathbf{k}) = \begin{pmatrix} 0 & 0 & 0 & e^{i\mathbf{k} \cdot \mathbf{a}_1} \\ 0 & 0 & e^{i\mathbf{k} \cdot \mathbf{a}_1} & 0 \\ 0 & -e^{-i\mathbf{k} \cdot \mathbf{a}_1} & 0 & 0 \\ -e^{-i\mathbf{k} \cdot \mathbf{a}_1} & 0 & 0 & 0 \end{pmatrix}^{\oplus \xi_1} \oplus \begin{pmatrix} 0 & 0 & 0 & e^{i\mathbf{k} \cdot \mathbf{a}_2} \\ 0 & 0 & e^{i\mathbf{k} \cdot \mathbf{a}_2} & 0 \\ 0 & -e^{-i\mathbf{k} \cdot \mathbf{a}_2} & 0 & 0 \\ -e^{-i\mathbf{k} \cdot \mathbf{a}_2} & 0 & 0 & 0 \end{pmatrix}^{\oplus \xi_2} \quad (15)$$

This matrix is equivalent to the one in Eq.(2) with ( $\chi_1 = 2\xi_1$ ,  $\chi_2 = 2\xi_2$ ) Majorana modes. The orthogonal transformation between both can be absorbed in the Gaussian channel (and thus in  $X$ ) so that entangling Majoranas by placing them in their joint vacuum is indeed equivalent to entangling full virtual fermions in the more traditional way.

- [8] S. Bravyi, Quantum Info. Comput. **5**, 216238 (2005).
- [9] N. Schuch, M. M. Wolf, and J. I. Cirac, Proceedings on the conference on Quantum information and many body quantum systems, 129 (2008), arXiv:1201.3945.
- [10] An interesting difference between the 1d and the 2d case can also be noticed. Where Pirvu *et al.* found a characteristic hump in the energy density error for intermediate system lengths in 1d critical systems [20], these humps

are completely absent in 2d. Note however that this could also be related to the Gaussian nature of the ansatz.

- [11] A. Cadarso, M. Sanz, M. M. Wolf, J. I. Cirac, and D. Pérez-García, Phys. Rev. B **87**, 035114 (2013), arXiv:1209.3898.
- [12] J. Dubail and N. Read, Physical Review B **92** (2015), 10.1103/physrevb.92.205307, arXiv:1307.7726.
- [13] N. Read, Phys. Rev. B **95**, 115309 (2017), arXiv:1608.04696.
- [14] T. B. Wahl, H.-H. Tu, N. Schuch, and J. I. Cirac, Physical Review Letters **111** (2013), 10.1103/physrevlett.111.236805, arXiv:1308.0316.
- [15] T. B. Wahl, S. T. Haßler, H.-H. Tu, J. I. Cirac, and N. Schuch, Phys. Rev. B **90**, 115133 (2014), arXiv:1405.0447.
- [16] S. Yang, T. B. Wahl, H.-H. Tu, N. Schuch, and J. I. Cirac, Physical Review Letters **114** (2015), 10.1103/physrevlett.114.106803, arXiv:1411.6618.
- [17] B. Béri and N. R. Cooper, Phys. Rev. Lett. **106**, 156401 (2011), arXiv:1101.5610.
- [18] S. Yin, N. R. Cooper, and B. Béri, Phys. Rev. B **99**, 195125 (2019), arXiv:1812.07417.
- [19] L. Fidkowski and A. Kitaev, Phys. Rev. B **81**, 134509 (2010), arXiv:0904.2197.
- [20] B. Pirvu, G. Vidal, F. Verstraete, and L. Tagliacozzo, Phys. Rev. B **86**, 075117 (2012), arXiv:1204.3934.

## Appendix A: Analytical proof for the fixed parity structure of GfPEPS

First consider the 1d case with  $f = \chi = 1$  so that  $A = \lambda J$  with  $J = \begin{pmatrix} 0 & 1 \\ -1 & 0 \end{pmatrix}$  (and  $J_n = J^{\oplus n}$ ). Because  $XX^T = 1$ ,  $AA^T + BB^T = 1$  implying that there exists a matrix  $O \in O(2)$  with  $B = \sqrt{1 - \lambda^2}O$ . Furthermore,  $AB + BD = 0$  so that  $D = -\lambda O^T J O = -\lambda \det(O)J$ . Consequently, the Fourier transformed correlation matrix of the GfPEPS in the high-symmetry points is given by

$$G_{\text{out}} = \lambda J + (1 - \lambda^2) (-\lambda J - O(\pm J)O^T)^{-1} \quad (A1)$$

with the plus sign in the zone center and the minus sign at  $k = \pi$ . Simplifying this further, one obtains

$$\begin{aligned} G_{\text{out}} &= \lambda J + (1 - \lambda^2) (-\lambda \mp \det(O))^{-1} J^{-1} \\ &= \lambda J + (1 - \lambda^2) (\lambda \pm \det(O))^{-1} J \\ &= \pm \det(O) J \end{aligned} \quad (\text{A2})$$

Making a  $\pi$  jump in Fourier space hence corresponds to an extra minus sign for the parity, which is in accordance with the odd number of virtual Majorana modes. Furthermore, the parity changing/conserving nature of the projection is determined by  $\det O$ . Writing  $X$  as  $\tilde{O}^T J_{f+\chi} \tilde{O}$ , it is straightforward to see that

$$\tilde{O} = \begin{pmatrix} 1 & & & \\ & \lambda & \sqrt{1-\lambda^2} & \\ & \sqrt{1-\lambda^2} & -\lambda & \\ & & & 1 \end{pmatrix} \begin{pmatrix} 1 & \\ & O \end{pmatrix} \quad (\text{A3})$$

and thus  $\text{Pf}(G_{\text{out}}) = (-1)^\chi \det \tilde{O} \text{Pf}(G_{\text{in}}) = (\mp 1)^\chi \det \tilde{O}$ . This can be generalized to all integer  $\chi$  by induction. Again starting from the purity of  $X$  and the fact that  $A = \lambda J$ , one obtains (e.g. utilizing the SVD of  $B$ ) that there exists an  $O \in O(2\chi)$  so that

$$X = \begin{pmatrix} 1 & \\ & O^T \end{pmatrix} \begin{pmatrix} \lambda J & \sqrt{1-\lambda^2} \\ -\sqrt{1-\lambda^2} & -\lambda J \\ & & J_{\chi-f} \end{pmatrix} \begin{pmatrix} 1 & \\ & O \end{pmatrix} \quad (\text{A4})$$

and thus  $X = \tilde{O}^T J_{f+\chi} \tilde{O}$  with  $\det \tilde{O} = -\det O$ . Using this orthogonal transformation, the correlation matrix of the output state can be rewritten as

$$G_{\text{out}} = \lambda J + (1 - \lambda^2) \begin{pmatrix} 1 \\ 0 \end{pmatrix}^T \left( \begin{pmatrix} -\lambda J & \\ & J_{\chi-f} \end{pmatrix} \mp X' \right)^{-1} \begin{pmatrix} 1 \\ 0 \end{pmatrix} \quad (\text{A5})$$

where  $X' = O J_\chi O^T = \begin{pmatrix} A' & B' \\ -B'^T & D' \end{pmatrix}$  can be interpreted as a new but lower-dimensional GfPEPS parameter matrix with  $X' X'^T = 1$ . Using the definition of Schur complements this can be simplified further to

$$G_{\text{out}} = \lambda J \mp (1 - \lambda^2) (\pm \lambda J + G')^{-1} \quad (\text{A6})$$

with  $G' = A' + B'(D' \mp J_{\chi-f})^{-1} B'^T$ . Assuming validity of the fixed parity configuration for  $\chi - 1$ ,  $G' = (\mp 1)^{\chi-1} \det O J$  yielding

$$\begin{aligned} G_{\text{out}} &= \lambda J + (1 - \lambda^2) J (\lambda - (\mp 1)^\chi \det O)^{-1} \\ &= \lambda J - J (\lambda - (\mp 1)^\chi \det \tilde{O}) \\ &= (\mp 1)^\chi \det \tilde{O}. \end{aligned} \quad (\text{A7})$$

Extending the proof to higher dimensions proceeds along similar lines but with  $G_{\text{in}}$  now existing of  $J$  blocks with possibly different signs (let  $\phi$  denote the number of

$-J$  blocks). For the output correlation matrix, one then obtains

$$G_{\text{out}} = \lambda J - (1 - \lambda^2) \begin{pmatrix} 1 \\ 0 \end{pmatrix}^T \left( \begin{pmatrix} \lambda J & \\ & -J_{\chi-f} \end{pmatrix} + X' \right)^{-1} \begin{pmatrix} 1 \\ 0 \end{pmatrix} \quad (\text{A8})$$

but now with  $\chi = \sum_i \chi_i$  and  $X' = O G_{\text{in}} O^T = O' J_\chi O'^T$  so that  $\det O = \det O' (-1)^\phi$ . Again simplifying this further yields

$$G_{\text{out}} = \lambda J - (1 - \lambda^2) (\lambda J - G')^{-1} \quad (\text{A9})$$

where validity of the proposition for  $\chi - 1$  can again be used to rewrite  $G'$  as  $(-1)^{\chi-1} \det O' J$  so that

$$\begin{aligned} G_{\text{out}} &= \lambda J + (1 - \lambda^2) J (\lambda - (-1)^{\chi-1} (-\det \tilde{O} (-1)^\phi))^{-1} \\ &= \lambda J - J (\lambda - (-1)^{\chi-\phi} \det \tilde{O}) \\ &= (-1)^{\chi-\phi} \det \tilde{O}. \end{aligned} \quad (\text{A10})$$

Indeed, this result corresponds to the expected extra factor  $(-1)^{\chi_i}$  for a  $\frac{\chi_i}{2}$  jump in Fourier space, thus completing the proof.

Finally, the proof can be extended to multiple physical fermions by first transforming  $A$  to  $\bigoplus_{j=1}^f \lambda_j J$  with  $O_1 \in O(2f)$ . Purity of  $X$  in combination with the SVD of  $B$  can then again be used to construct  $O_2 \in O(2\chi)$  with

$$X = O^T \begin{pmatrix} (\lambda_j J)^\oplus & \sqrt{1-\lambda_j^2}^\oplus \\ -\sqrt{1-\lambda_j^2}^\oplus & -(\lambda_j J)^\oplus \\ & & J_{\chi-f} \end{pmatrix} O \quad (\text{A11})$$

and  $O = \begin{pmatrix} O_1 & \\ & O_2 \end{pmatrix}$ . For the output parity this gives

$$\begin{aligned} \text{Pf}(G_{\text{out}}) &= \det O_1 \text{Pf} \left[ (\lambda_j J)^\oplus \right. \\ &\quad \left. - \sqrt{1-\lambda_j^2}^\oplus ((\lambda_j J_j)^\oplus - G')^{-1} \sqrt{1-\lambda_j^2}^\oplus \right] \end{aligned} \quad (\text{A12})$$

with again  $G' = A' + B'(D' - J_{\chi-f})^{-1} B'^T$  and  $X' = O_2 G_{\text{in}} O_2^T$ . As the calculation of the inner inverse is no longer analytically possible since  $f > 1$ , we rewrite the Pfaffian, using its Schur complement properties

$$\begin{aligned} \text{Pf}(G_{\text{out}}) &= \det O_1 \text{Pf}^{-1} \left( (\lambda_j J_j)^\oplus - G' \right) \\ &\quad \text{Pf} \left( \begin{pmatrix} (\lambda_j J_j)^\oplus & \sqrt{1-\lambda_j^2}^\oplus \\ -\sqrt{1-\lambda_j^2}^\oplus & (\lambda_j J_j)^\oplus - G' \end{pmatrix} \right) \end{aligned} \quad (\text{A13})$$

where the Pfaffian of the large matrix can be calculated via its minors and making use of the validity of the proposition for lower  $\chi$ .

## Appendix B: Optimization algorithm

In this paper, the energy density was used as a cost function for the variational optimization of GfPEPS. Not only does this allow the calculation of exact gradients (which is indispensable for a stable and reproducible optimization of the critical models under consideration), it can also deal with models for which the exact solution is not known analytically (e.g. when an elevated number of physical fermions is considered). The energy density function of a GfPEPS with respect to a general, quadratic and translation invariant Hamiltonian as in Eq. (11) can be expressed as

$$\begin{aligned}
 e &= \frac{1}{N} \langle H_{\text{BdG}} \rangle \\
 &= \frac{1}{2N} \sum_{\mathbf{k}} \langle \Upsilon_{\mathbf{k}}^\dagger H_{\text{BdG}}(\mathbf{k}) \Upsilon_{\mathbf{k}} \rangle + \frac{\tilde{E}}{N} \\
 &= \frac{i}{2N} \sum_{\mathbf{k}} \text{Tr} \left( \tilde{H}_{\text{BdG}}(\mathbf{k}) G_{\text{out}}(\mathbf{k}) \right) + \frac{\tilde{E}}{N}
 \end{aligned} \tag{B1}$$

where  $\tilde{H}_{\text{BdG}}(\mathbf{k}) = \left( V^{-1\dagger} H_{\text{BdG}}(\mathbf{k}) V^{-1} \right)^T$  with  $H_{\text{BdG}}(\mathbf{k}) = \begin{pmatrix} \Xi(\mathbf{k}) & \Delta(\mathbf{k}) \\ -\Delta^*(-\mathbf{k}) & -\Xi^T(-\mathbf{k}) \end{pmatrix}$  and with the matrix  $V$  again transforming the Fourier space Nambu spinor into the  $d_{\mathbf{k}}^i$  operators. Note that the energy density is linear in the GfPEPS correlation matrix. The variational parameters are collected in the matrix  $X^{\text{loc}} \in \mathbb{R}^{2(f+\chi_1+\chi_2) \times 2(f+\chi_1+\chi_2)}$ , describing the transformation between  $G_{\text{in}}(\mathbf{k})$  and  $G_{\text{out}}(\mathbf{k})$ . In case of a pure state, this matrix satisfies  $X^{\text{loc}} X^{\text{loc}\dagger} = \mathbb{1}$  so that it can be parameterized as  $X^{\text{loc}} = Q^T J_{f+\chi_1+\chi_2} Q$  with  $Q \in O(2(f+\chi_1+\chi_2))$ . By replacing  $J$  blocks in  $J_{f+\chi_1+\chi_2}$  by their transpose, it is possible to construct both parity conserving and changing  $\mathcal{E}$  projections with a  $Q \in SO(2(f+\chi_1+\chi_2))$ , yielding a  $(2(f+\chi_1+\chi_2)-1)(f+\chi_1+\chi_2)$ -dimensional variational manifold. On this manifold, a Riemannian limited memory quasi-Newton (L-BFGS) procedure was applied to find the minimum of  $e(X)$ , starting from a random initial guess. Analytic gradients were computed via the chain rule applied to Eq. (B1).

In the main text, we mentioned that non-trivial optimization paths have to be followed to derive the results in Fig. 2-5. Indeed, the high level of criticality in the models combined with inadmissible Fermi surfaces

typically results in challenging optimization problems where a stabilizing alteration to the Hamiltonian is necessary to attain reproducible results. In the 1d case of the Kitaev chain, these problems are relatively under control, especially for odd  $\chi$ . Therefore, the ground state can be approximated with GfPEPS directly in the critical point as well as in the chiral and trivial phases. In the 2d square lattice hopping model, on the other hand, one should start from the anisotropic variant of the system (we typically started from  $\frac{t_y}{t_x} = 2$ ), apply GfPEPS hereto and use the optimal  $X^{\text{loc}}$  as an initial guess for a slightly lower  $\frac{t_y}{t_x}$ . Systematically decreasing the anisotropy in this way, the isotropic point can be probed without encountering parity obstructions. This procedure was repeated for all system sizes and bond dimensions. Once the energy density error started to flatten out as a function of the system size (signaling that the thermodynamic limit is reached), GfPEPS for even larger system sizes were directly optimized in the isotropic point with the optimal  $X^{\text{loc}}$  from the smaller system size as an initial guess. GfPEPS optimizations for the Chern insulator model with one Dirac cone can also be performed directly in the critical point and no stabilizing alterations have to be taken into account. For the point with two Dirac cones, on the other hand, it is beneficial to approach the critical point from inside the chiral phase. We started from  $\Delta = 1$  and systematically decreased  $\Delta$  to zero with the previous optimum as the new initial guess. While this method may not always yield the *minimum minimorum* for the energy density, the results for  $\Delta e$  are reproducible and correspond to a power law decrease as a function of the bond dimension.

Finally we also comment on some other variations of the optimization method. Simulations can, for instance, be performed at elevated temperatures, utilizing a mixed GfPEPS ansatz where  $X^{\text{loc}} X^{\text{loc}\dagger} < \mathbb{1}$ . This can be enforced by taking  $X^{\text{loc}} = \tan Q$  with  $Q$  anti-symmetric (again resulting in a  $(2(f+\chi_1+\chi_2)-1)(f+\chi_1+\chi_2)$ -dimensional variational manifold). Not only does this approach complicate the expressions for the analytic gradient of the energy density, the thermodynamic cost function should also be replaced by the free energy density, thus adding an entropic contribution to the cost function. Especially the latter becomes significantly more complicated to compute. Therefore, one might resort to cost functions directly expressing the distance between the exact and the GfPEPS correlation matrices. However, the determination of analytic gradients should also be possible for these cost functions, for instance, precluding trace norm distances in most cases.